Straightforward access to mono- and bis-cycloplatinated helicenes that display circularly polarized phosphorescence using crystallization resolution methods

Chengshuo Shen,[a] Emmanuel Anger,[a] Monika Srebro,[b] Nicolas Vanthuyne,[c] Kirandeep K. Deol,[d] Truman D. Jefferson Jr.,[d] Gilles Muller,[d] J. A. Gareth Williams,[e] Loïc Toupet,[a] Christian Roussel,[c] Jochen Autschbach,[f] RégisRéau,[a] and Jeanne Crassous[a]

Enantiopure mono-cycloplatinated-[8]helicene and bis-cycloplatinated-[6]helicene derivatives were prepared through column chromatography combined with crystallization of diastereomeric complexes using a chiral ancillary sulfoxide ligand. The UV-visible spectra, circular dichroism, molar rotations, and (circularly polarized) luminescence activity of these new helical complexes have been examined in detail and analysed with the help of first-principles quantum-chemical calculations.

Introduction

Helicenes are among the rare classes of molecules displaying exceptionally strong chiroptical properties (optical rotation, circular dichroism into the visible region), thanks to their inherent helical chirality combined with extended π-conjugation.[1] Structural and electronic features provide helicenes with additional properties that are essential for the development of chiral molecular materials and devices.[2] For instance, helicenes have been reported displaying circularly polarized luminescence (CPL),[3a-d] redox[3e-g] or optical switching,[3h,i] electrical conductivity,[3j,k] non-linear optical (NLO) activity,[3l] to name a few. The conception of new chiral materials and devices is closely related to efficient and innovative synthetic and enantiomer-resolution methods allowing not only structural diversity but also gram-scale synthesis. We have recently demonstrated the potential of the organometallic approach to prepare the first metallahelicenes bearing a metal ion incorporated into the helical backbone.[4] We have shown that using a 3rd row transition-metal ion, this strategy confers multifunctionality on the helicene, by combining the chiroptical properties with room temperature phosphorescence and redox activity.

Apart from HPLC and column chromatographic separations,[1,5a,b] the few known preparations of enantiopure helicene derivatives are essentially based on asymmetric synthesis using either a chiral catalyst,[5c,d] kinetic resolution,[5e] enantio-[5f] or diastereoselective syntheses.[5g,h] Although the parent carbo[n]helicenes have been known to form conglomerates,[6a] resolution of helicene enantiomers by crystallization methods is rarely used.[6b-e]

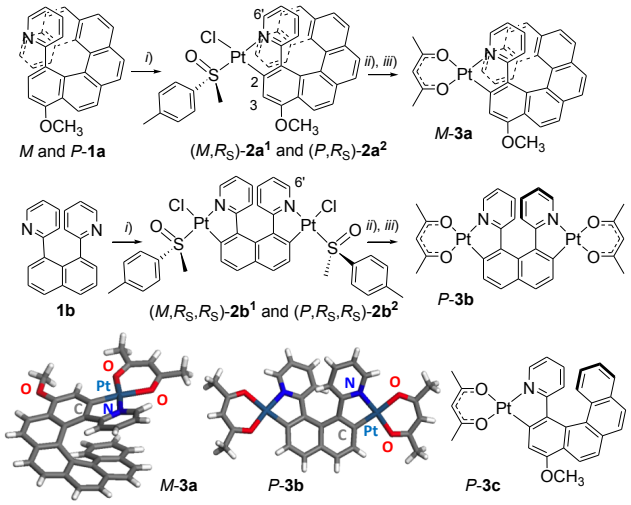

Scheme 1. General synthesis of enantiopure Pt-[8]helicene and Pt_2-[6]helicene derivatives *M*-**3a** and *P*-**3b** from (±)-**1a** and **1b** respectively. *i*) (S_s,S_s)-$PtCl_2$(*p*-tolyl-MeSO)$_2$, toluene, Na_2CO_3, Ar, reflux, overnight, 60%; *ii*) column chromatography and/or crystallization; *iii*) pentane-2,4-dione, toluene, Na_2CO_3, Ar, reflux, 2 h. X-ray crystallographic structures of **3a** and **3b** (one enantiomer shown) and chemical structure of **3c**.[4a,b]

In this paper, we describe a straightforward access to the unprecedented mono-platina[8]helicene (**3a**) and bis-platina[6]helicene (**3b**) (Scheme 1). These new complexes were obtained in enantiopure forms through simple crystallization of diastereomeric complexes {(*M**,R_S)-**2a**^{1,2} and (*M**,R_S,R_S)-**2b**^{1,2}, respectively} bearing a chiral ancillary sulfoxide ligand, which was then replaced by the achiral acetylacetonate (acac) ligand.

The chiroptical properties (circular dichroism and molar rotations), and the photophysical properties (UV-visible absorption, non-polarized and circularly-polarized luminescence) of the complexes are examined and analyzed with the help of quantum-chemical calculations in the context of parameters including the size of the helicene, the helicity, and the role of the metal ions within the helicene.

B Results and discussion

B.1. Synthesis and solid state structure

Phenylpyridine ligands are known to form stable platinacycles bearing a variety of ancillary ligands, including monodentate sulfoxides.[7] In a few examples, the sulfoxide ligand is a chiral one (usually *R*- or *S*-methyl-*p*-tolyl-sulfoxide) and therefore leads to enantiopure chiral cycloplatinated complexes.[8] Using this methodology, the diastereomeric mixture of monoplatinated [8]helicenes (*M*,R_S)-**2a**^{1} and (*P*,R_S)-**2a**^{2} were prepared in one step by orthoplatination of racemic 2-pyridyl-[6]helicene[4d] **1a** using (S_S,S_S)-$PtCl_2$(*p*-tolyl-MeSO)$_2$ (*trans/cis* mixture) as the enantiopure platinum source (*ee*>97%), in refluxing toluene and under basic conditions (Na_2CO_3). This cycloplatination reaction increases the size of the helicene from a hexa- to an octahelicene derivative. The presence of two (*M*,R_S)-**2a**^{1}and (*P*,R_S)-**2a**^{2} diastereomers is ascertained by ^{1}H and ^{13}C NMR spectra which show the presence of two sets of signals in a 1:1 ratio. Compared to the non-metallated ligand **1a**, complexes **2a**^{1,2} display well-resolved ^{1}H NMR spectra in which ^{195}Pt-^{1}H couplings constants are observed (**2a**^{1}: 34 Hz for H$^{6'}$ and 52 Hz for H^3, see ESI†).

Gratifyingly, crystallization by slow diffusion of pentane vapour into a CH_2Cl_2 solution yielded single crystals of the pure diastereomer (*M*,R_S)-**2a**^{1}. The X-ray crystallographic structure ($P2_1$ space group, Figure 1) clearly depicts (*i*) the eight ortho-fused cycles with the platinacycle incorporated within the helical backbone with a helicity (dihedral angle between terminal rings) of 11.42°, a value which is very low due to intramolecular π–π stacking (centroid-to-centroid distances of 3.465 Å between the pyridyl ring and the 7th benzene ring); (*ii*) the sulfoxide and chloride disposed *trans* to the N and C atoms respectively, due to the strong *trans* influence of the latter; and (*iii*) the *M* and the R_S configurations only. Note that the sulfoxide ligand is coordinated through the S atom and that the *p*-tolyl group is directed away from the helicene. Another important feature is the columnar packing of the molecules along the *x* axis arising from intermolecular π–π stacking between adjacent helicene moieties (*vide supra*, Figure 1). Such a supramolecular arrangement may be the driving force for the efficient diastereoselective crystallization process.

This encouraging result prompted us to conduct the separation of (*M*,R_S)-**2a**^{1} and (*P*,R_S)-**2a**^{2} diastereomers on a preparative scale. This was achieved by initial column chromatography (using heptane/ethyl acetate 3:1 as the eluent) to obtain partially resolved samples, which subsequently crystallized out of solution as enantiomerically and diastereomerically pure (*M*,R_S)-**2a**^{1} and (*P*,R_S)-**2a**^{2} in 33 and 18% yield respectively. Single crystals of (*P*,R_S)-**2a**^{2} suitable for X-ray diffraction analysis were grown from the heptane/ethyl acetate solution. The X-ray crystallographic structure of (*P*,R_S)-**2a**^{2} (Figure 1) displayed the same features as for (*M*,R_S)-**2a**^{1} except that (*i*) the helicene has its configuration inverted and is directed towards the *p*-tolyl substituent, and (*ii*) no supramolecular organization is observed.

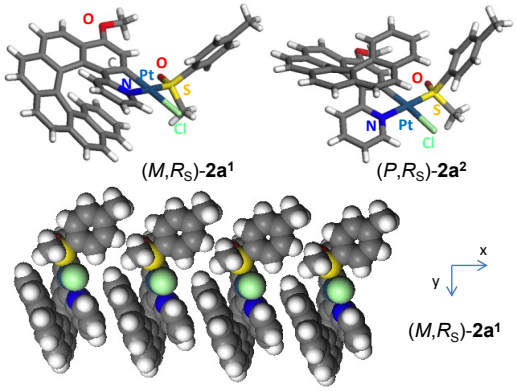

Figure 1. X-ray crystallographic structures of diastereomerically pure Pt-[8]helicene derivatives (*M*,R_S)-**2a**^{1} and (*P*,R_S)-**2a**^{2}. Columnar packing of (*M*,R_S)-**2a**^{1} along the *x* axis (CPK model representation).

In a final step, the chloride ligand and the *p*-tolyl methyl sulfoxide used as a chiral auxiliary agent were replaced by a bidentate acetylacetonate ligand, giving rise to the enantiomeric pair *M*- and *P*-**3a** (Scheme 1) in 95% yield. Note that no racemization was observed during this step since the molecules are stable in refluxing toluene. The X-ray structure of **3a** obtained from a racemic sample is displayed in Scheme 1. It shows that the Pt(II) complex **3a** is a structural analogue of a carbo[8]helicene with a small helicity (15.04°) due to the strong intramolecular π–π interaction.

Since we have demonstrated that diastereomeric resolution by column chromatography coupled with crystallization is a convenient way for producing enantiopure helicene derivatives, enabling the preparation of enantiopure samples on a scale of several hundred milligrams (see ESI), a straightforward synthesis of a [6]-helicene incorporating *two* platinum centres was performed by taking advantage of the fact that cycloplatination increases the helicene size by two fused rings. Indeed, the first bis-cycloplatinated [6]helicene derivative was prepared in enantiopure form in only three steps through the double cycloplatination of a 1,8-bisarylnaphthalene scaffold.[9] The proligand 1,8-bis(2-pyridyl)naphthalene **1b** was prepared by a Stille coupling between 1,8-diiodonaphthalene and 2-(trimethylstannyl)-pyridine, according to a known procedure[9c,e] (see ESI). 1,8-Bis-aryl-naphthalene derivatives are known to display *cis-trans* isomerism, due to steric hindrance of the aryl groups that are forced into close proximity by the naphthalene platform. While the *cis*-form is centrosymmetric, the *trans*-form is C_2-symmetric and exists as two enantiomers.[9]

Proligand **1b** crystallizes in a non-centrosymmetric space group ($P2_1$), where the two pyridyl groups are transoid and

twisted with a dihedral angle of 35.44° (Figure 2), with weak π–π interaction observed (centroid-centroid distance = 3.683 Å). While molecule **1b** adopts a helical shape in the solid state, it is conformationally labile in solution and is overall achiral. The double orthometallation of **1b** was then accomplished by reaction with 2 equiv of (R_S,R_S)-PtCl$_2$(*p*-tolyl-MeSO)$_2$ (*trans/cis* mixture) as an enantiopure platinum source in refluxing toluene in the presence of a base (Na$_2$CO$_3$). The ^{1}H NMR and ^{13}C NMR spectra of the product of this reaction revealed the presence of a mixture of two bis-cyclometallated compounds (**2b^1** and **2b^2**) in the ratio 1.5:1 respectively, based on integration of the H^6-py proton (see ESI) in the 9–10 ppm region of the ^{1}H NMR spectrum.

Slow crystallization by diffusing pentane vapour over a CHCl$_3$ solution yielded single crystals that were identified as the pure diastereomer (*P*,R_S,R_S)-**2b^2** by X-ray crystallography. Indeed, the solid state structure ($P2_12_12_1$ space group) shows that the bis-Pt(II) complex **2b^2** adopts a helical topology (Figure 2), with a helicity angle between the two terminal pyridyl groups of 58.8°, in very good agreement with mono-platina[6]helicenes and carbo[6]helicene derivatives.[4] In this unprecedented structure, two almost planar platinacycles (dihedral angles between phenyl and pyridyl rings < 19°) are incorporated within the helical backbone (with the two Cl *trans* to the metallated carbon atoms and two *S*-sulfoxides *trans* to the N atoms). A supramolecular columnar arrangement is also present in the solid state due to intermolecular π–π stacking between adjacent helicene moieties (Figure 2). Clearly, bis-metallahelicene derivatives can be straightforwardly produced by double orthometallation of a bis-substituted naphthalene platform. Furthermore, given the 1.5:1 diastereomeric ratio of (*M*,R_S,R_S)-**2b^1** and (*P*,R_S,R_S)-**2b^2**, the C–H activation that occurs during the cycloplatination appears to be diastereoselective.[4d,10] Despite the moderate efficiency, such diastereoselectivity is very rare in cycloplatination reactions since high *ee* values are difficult to achieve when high-temperature reactions are required (refluxing toluene here).

Based on the successful isolation of enantiomerically and diastereomerically pure single crystals of (*P*,R_S,R_S)-**2b^2**, the preparative resolution of **2b^{1,2}** was studied by taking advantage of their different solubilities. This was accomplished by simply using the appropriate quantity of heptane/CHCl$_3$ (3:1) as the crystallization solvent: (*P*,R_S,R_S)-**2b^2** precipitated in 34% yield, whereas the mother liquors contained mainly (*M*,R_S,R_S)-**2b^1**, which was finally obtained in pure form by column chromatography (SiO$_2$, EtOAc as the eluent) followed by crystallization in heptane/CHCl$_3$ (3:1) (33% yield). The mirror-image experiment starting from (S_S,S_S)-PtCl$_2$(*p*-tolyl-MeSO)$_2$ yielded pure (*M*,S_S,S_S)-**2b^1** and (*P*,S_S,S_S)-**2b^2**. In a final step, the chloride and sulfoxide ligands were replaced by acac, yielding enantiomeric pairs *M*- and *P*-**3b** (Scheme 1). The X-ray structure shows that **3b** has the same helicity (51.24°) as the former monoplatina[6]helicene analogue **3c** (52.3°),[4a] but a more open skeleton and therefore is more prone to racemization. This was experimentally verified on complexes **2b^1** and **2b^2** that revealed 30% loss of diastereomeric purity after refluxing in toluene for 72 hours, while complex **3b** displays a long half-life (~19 days at 100°C, see ESI).

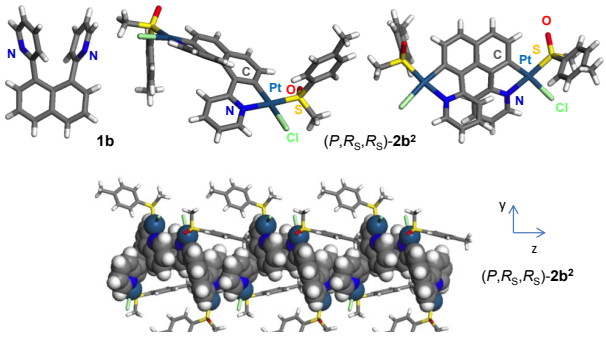

Figure 2. X-ray crystallographic structures of ligand **1b** and the pure diastereomeric complex (*P*,R_S,R_S)-**2b^1**. Columnar packing of (*P*,R_S,R_S)-**2b^1** is observed along the *z* axis (Pt$_2$-[6]helicene shown in CPK model representation).

B.2. Photophysical properties

Having to hand the different platinahelicene derivatives, with either different lengths (Pt-[6]-*vs.*Pt-[8]-helicene) or different numbers of Pt(II) atoms (Pt-[6]- *vs.* Pt$_2$-[6]-helicene), their absorption and photophysical properties were measured and compared. The UV-visible absorption data of compounds **1a**, **2a^{1,2}** and **3a** are summarized in Table 1 and the spectra are shown in Figure 3.

The electronic absorption spectrum of **1a** displays an intense high-energy band ($\varepsilon > 3 \times 10^4$ M^{-1} cm^{-1}) around 290 nm, with longer-wavelength shoulders and a tail out to 420 nm (Figure 3). This spectrum is typical of a [6]helicene derivative. The electronic absorption spectra of Pt-[8]helicene complexes **2a^{1,2}** and **3a** display several intense absorption bands between 250 and 380 nm and two weaker ($\varepsilon \sim$ 300–1000 M^{-1} cm^{-1}) lower-energy broad bands at 380 and 480 nm arising from interactions between the metal and the π-ligand. The absorption at these lowest energy bands in **2a^{1,2}** and **3a** are bathochromically shifted by ca. 50 nm compared to **1a** (*vide infra*). This red-shift is consistent with an elongation of the π-conjugated system from a [6]helicene to an [8]helicene via the ring closure that accompanies orthometallation (Scheme 1). UV-vis and CD spectra have been calculated by time-dependent DFT (TDDFT) at the BHLYP/SV(P) level (c.f. ESI),[11] see Figure 4, Tables 2 and 3. An excitation analysis in terms of MO-pair contributions of [6]helicene ligand **1a** shows that the main low-energy transitions are of π-π* type, with sizable dipolar oscillator strength values (e.g. excitation no. 3, Table 2,

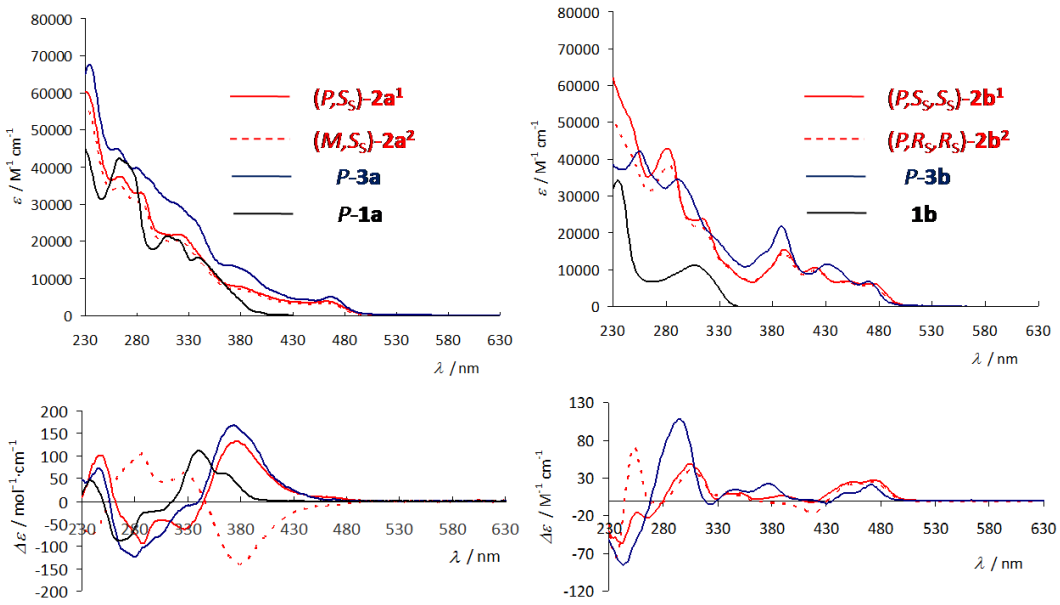

Figure 3.UV-vis and CD spectra of (*P*,S_S)-**2a**^{1}, (*M*,S_S)-**2a**^{2}, *P*-**3a**, (*P*,S_S,S_S)-**2b**^{1}, (*P*,R_S,R_S)-**2b**^{1}, and ***P***-**3b** in solution in dichloromethane at room temperature, compared to the starting organic ligands *P*-**1a** and **1b**.

Figure 4). In the case of **2a**^{1} and **3a**, the excitations at lower energy are assigned predominantly as HOMO-LUMO (*P*-**2a**^{1}, 84%; *P*-**3a**, 81%) (excitations no. 1, Table 2, Figure 4) and may be considered as a π-π* transitions localized in the N^C ligand system with some participation of the platinum 5*d* orbitals. The calculations therefore show that the orbitals of the metal centre efficiently interact with those of the helicoidal π-system.

Similarly, whilst the starting proligand **1b** displays two bands of moderate intensity at 233 nm ($\varepsilon \sim 34 \times 10^3$ M^{-1} cm^{-1}) and 303 nm ($\varepsilon \sim 11 \times 10^3$ M^{-1} cm^{-1}), the electronic absorption spectra of its Pt_2-[6]helicene complexes **2b**^{1,2} and **3b** show much more intense absorption between 250 nm and 350 nm (Figure 3), and three lower-energy, broad bands between 380 and 500 nm originating from the interaction between the two metallic ions and the π-ligand (*vide infra*). This strong modification and red-shift of the UV-vis spectra show the efficiency of the double orthometallation ring closure in creating elongated helical π-conjugated [6]helicene frameworks. Furthermore, metal-to-ligand charge transfers are more efficient when two metal centres are involved within the π-ligand. For example, comparing **3b** with the mononuclear Pt-[6]helicene **3c** (Table 1), it is apparent that the absorption bands in the visible region are not only shifted to lower energy in the dinuclear compounds, but that their molar absorptivity is also increased (e.g. ε values at 434 ± 1 nm are 11200 and 7110 $M^{-1}cm^{-1}$ for the di- and mononuclear compounds respectively). A similar red-shift has been observed recently when the bridging unit is a heterocycle, for example, in diplatinum complexes of diphenylpyrazines and 2,3-diphenylpyrimidines.[12] Typically, in cycloplatinated complexes of arylpyridine ligands, electrochemical studies and first-principles theory indicate that the HOMO is predominantly localised on the metallated ring and the metal ion, whereas the LUMO resides primarily on the pyridyl rings.[13] In organometallic helicenes **2b**^{1,2} and **3b**, the metal atom functions not only to construct the helicoidal framework by double orthometallation (Scheme 1) but also to impact markedly the electronic properties of the π-conjugated system. Indeed, the excitations at lower energy are assigned to HOMO-LUMO (*P*-**2b**^{1}, 94%; *P*-**3b**, 93%) (see excitations no. 1, Figure 4 and Table 3). This excitation can be considered as a π-π* transition localized in the π-ligand with non-negligible involvement of metal orbitals. The same type of excitation can be also found in the case of the mono-platinum

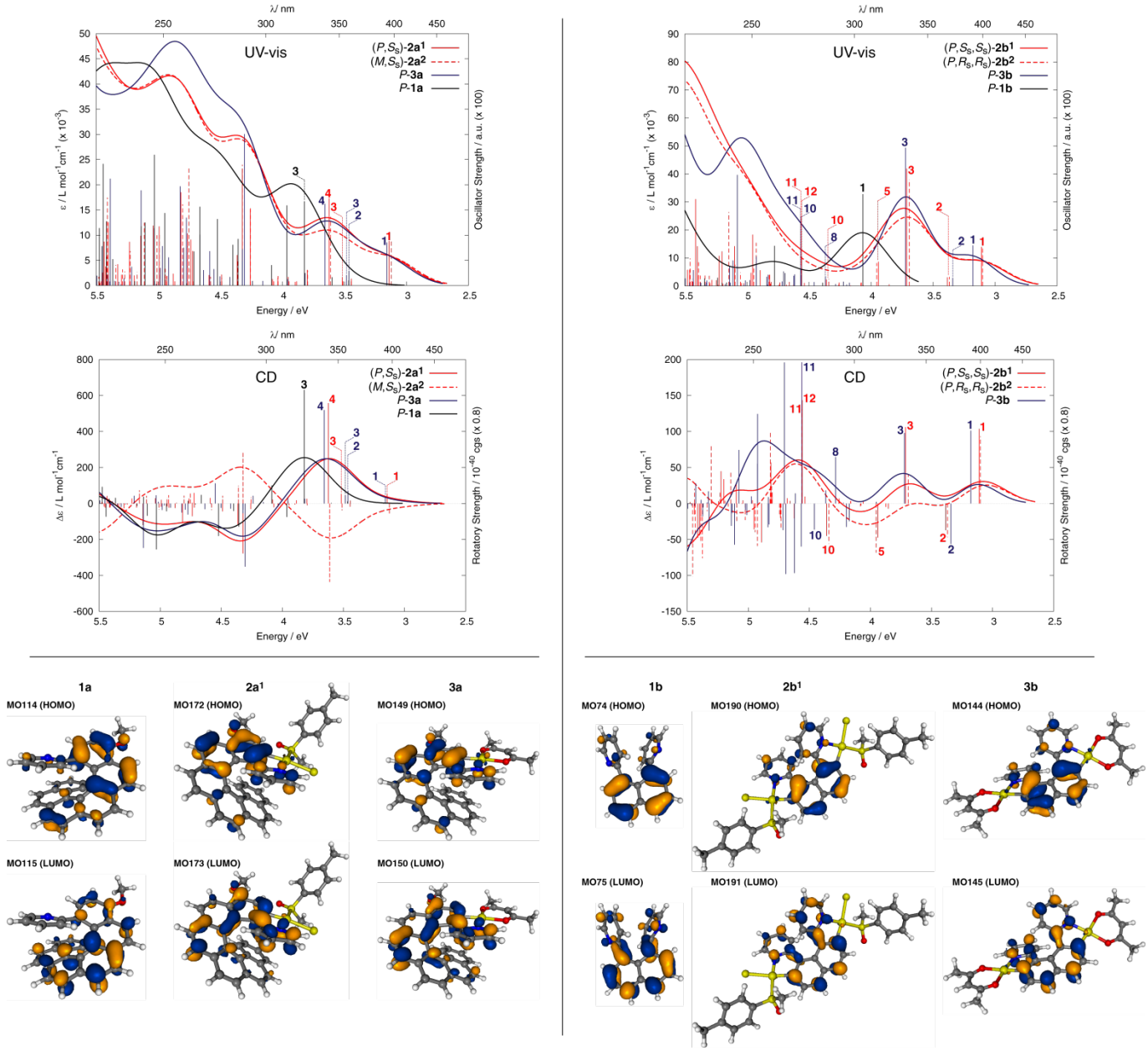

Figure 4. Upper panels: Comparison of the calculated UV-vis (top) and CD spectra (bottom) of *P*-**1a**, *P*-**3a**, (*P*,S_S)-**2a**^{1} and (*M*,S_S)-**2a**^{2} (left) and *P*-**1b**, *P*-**3b**, (*P*,S_S,S_S)-**2b**^{1} and (*P*,R_S,R_S)-**2b**^{2} systems (right). Color and line schemes correspond to those in Figure 3. No spectral shifts were applied. Numbers correspond to excitations that were analyzed in detail. Lower panels: Isosurface plots of the HOMO and LUMO of series **1a**, **2a**^{1}, and **3a** and of series **1b**, **2b**^{1}, and **3b** are shown. Further details are provided in the ESI.

complex **3c** but with much weaker intensity.[4a,b] Accordingly, higher dipolar strengths of this transition in (**2b**/**3b**) may be attributed to the presence of two Pt centers built into the N^C π-system and modifying the electronic properties of the helicene platform compared to **3c**.

To summarize: A direct comparison of the UV-vis spectra of **1a** and **3a-c** (Figure 5) along with an analysis of the calculated spectra highlights the differences and common features shared by these four helicene systems: *i*) additional low-energy HOMO-LUMO transitions present in cycloplatinated helicenes **3a-c** with non-negligible involvement of Pt orbitals that are not present in organic helicene **1a**; *ii*) similar UV-vis spectra of Pt-[8]helicene **3a**, Pt_2-[6]helicene **3b**, and Pt-[6]helicene **3c** reflecting an extended π-conjugation involving one or two Pt atoms.

Interactions between the metal and the π-ligands are not only responsible for the intense, low-energy absorbance in the UV-vis spectra but also for dramatic differences in the emission properties of these new platinahelicenes compared to the metal-free proligands. Proligand **1a** exhibits the typical emission behaviour of organic π-conjugated systems.[4b] In dichloromethane solution at room temperature, it displays

structured blue fluorescence around 430 nm (Φ = 3.3%, τ = 5.9 ns; see Table 1 and Figure 6). At 77K, the fluorescence is only

Table 1. Photophysical data of ligand **1a** and of the Pt^{II}-helicene complexes **2a**[1], **3a**,**b**, together with that of the parent Pt-[6]helicene **3c** for comparison.

	1a	**2a**[1]	**3a**	**3b**	**3c**[(f)]
Absorption λ_{max} / nm (ε /$M^{-1}cm^{-1}$) [(a)]	232 (43400), 265 (40800), 310 (21600), 339 (15600), 399sh (1280), 422 (760)	233 (66100), 263 (40900), 282 (37100), 320 (24100), 378 (8700), 466 (4340)	260 (49900), 281 (45400), 318sh (34300), 369 (15000), 467 (5320)	255 (42000), 290 (34200), 389 (21400), 433 (11200), 471 (6640)	255 (61300), 294 (34000), 316 (33500), 346 (3350), 435sh (7110), 452 (7800)
Emission λ_{max} / nm (298K) [(a)]	430, 453	677	648	633, 673	644
$\Phi_f \times 10^2$ (298 K) [(b)]	3.3	4.1	5.6	13	10
τ_{lum} / ns (298 K) deg. [aer.] [(c)]	5.9	24000 [780]	16500 [630]	18700 [970]	21000
k_Q^{O2} / 10^8 $M^{-1}s^{-1}$ [(d)]		5.6	6.9	4.4	
Emission λ_{max} / nm (77 K) [(e)]	420, 446, 474, 504 (fluo) 541, 589, 639 (phos)	641, 677	598, 644	608, 664, 727	592, 638, 691(sh)
τ_{lum} (77 K)	8.9 ns (fluo) 1.1 s (phos)	61 µs	32 µs	28 µs	45 µs

[(a)] In CH_2Cl_2 at 298 K. [(b)] Measured using $[Ru(bpy)_3]Cl_2$ as the standard. [(c)] Values in air-equilibrated solution in parentheses. [(d)] Bimolecular rate constant for quenching by O_2. [(e)] In diethyl ether / isopentane / ethanol (2:2:1 v/v). [(f)] Data from references 4a,b.

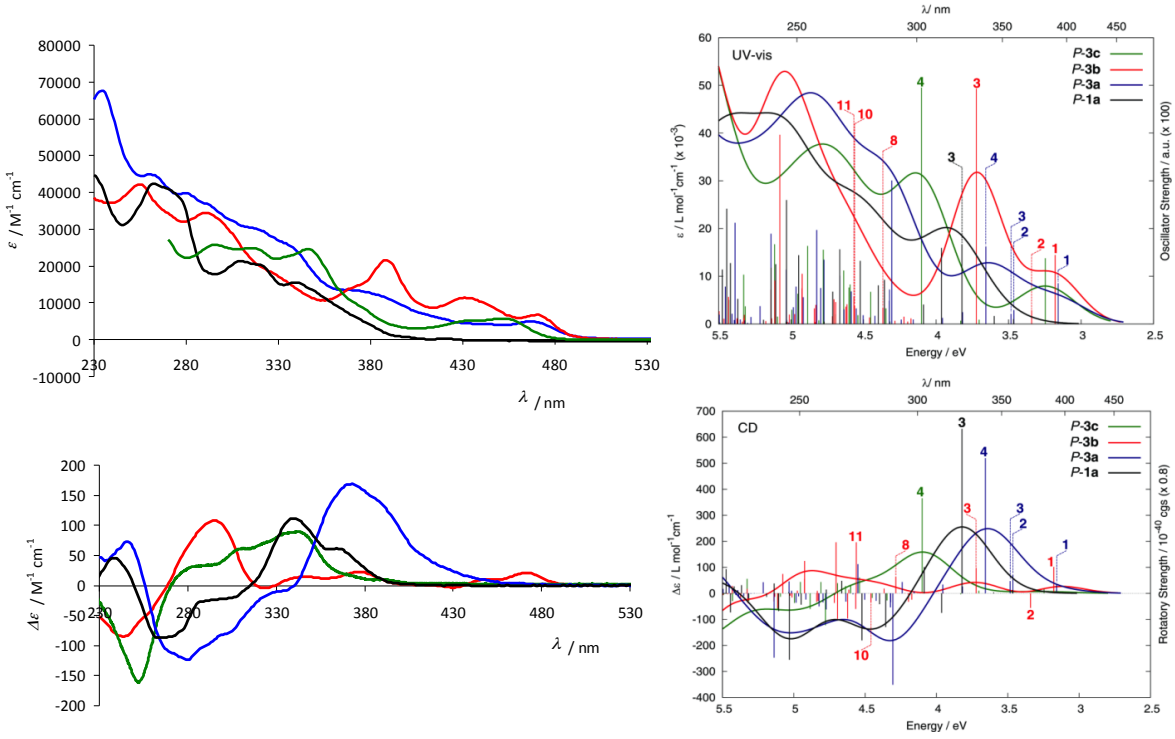

Figure 5. Comparison of the experimental (left) and calculated (right) UV-vis (top) and CD spectra (bottom) of *P*-**1a** (black line), *P*-**3a** (blue line), *P*-**3b** (red line), and *P*-**3c** (green line). No spectral shifts were applied in the calculated spectra. Numbers correspond to excitations that were analyzed in detail.

slightly blue-shifted but is then accompanied by a very long-lived green phosphorescence around 540 nm emanating from the triplet state (τ = 1.1 s), with similar vibrational structure to the fluorescence ($\Delta\nu \sim 1300$ cm^{-1}) (see ESI). As usual for such organic molecules, the phosphorescence is not observable at room temperature, the radiative rate constant being too small to compete with non-radiative decay processes.

When the platinum(II) ion is incorporated into the π-conjugated system, the emission properties change drastically. The platinahelicenes show no fluorescence but instead display strong room-temperature phosphorescence. As found in simpler complexes of arylpyridines, efficient spin-orbit coupling of the metal ion valence orbitals promotes very rapid intersystem crossing to the triplet state, eliminating the fluorescence from the S_1 state that was seen for the proligand, whilst facilitating the subsequent $T_1 \rightarrow S_0$ phosphorescence transition. Phosphorescence can then successfully compete with triplet non-radiative decay pathways even at room temperature. Indeed, platinahelicenes **2a**[1] and **3a** are efficient deep-red phosphors, with emission maxima of 677 and 648 nm respectively, and quantum yields of around 5% in deoxygenated solution at room temperature (Figure 6 and Table 1). The luminescence lifetimes of around 20 μs are, however, somewhat longer than those found for complexes of simpler arylpyridine ligands such as phenylpyridine,[13] likely because the metal ion has a proportionately smaller influence in the excited state extended over a larger π–system.

The presence of the second platinum centre is seen to slightly stabilise the triplet excited state of the diplatinum complex **3b** compared to the mononuclear Pt-[6]helicene **3c** (λ_{max} = 608 and 592 nm respectively at 77K), although an apparently larger stabilising effect of the solvent in the latter case leads to very similar spectra at room temperature. The phosphorescence quantum yield Φ of the dinuclear complex is slightly higher, though since the difference is close to the uncertainty on the measurement of Φ, it is not possible to make any definitive conclusions as to whether the presence of a second Pt ion leads to more efficient spin-orbit coupling pathways.[12] The phosphorescence quantum yield of Pt-[8]helicene **3a**, on the other hand, is lower than the analogous Pt-[6]helicene **3c** and the lifetime somewhat shorter. This might reflect an increased scope for non-radiative decay in the more extended structure of the [8]helicene, though again the differences are too small to draw firm conclusions.

As seen in Table 4 below, quantum-chemical calculations of luminescence properties for **1a**, and **3a**,**b**,**c** support the assignment: the calculated fluorescence and phosphorescence energies (2.9 eV and ~1.7 eV, respectively) of [6]helicene ligand **1a** correspond well to the experimental low-temperature results. Similarly, in the case of Pt complexes **3a**,**b**,**c** the calculated emission energies $S_1 \rightarrow S_0$ (~2.9 eV) were found to be very different from the measured luminescence values, while the energies of $T_1 \rightarrow S_0$ phosphorescence transitions (~ 1.9 eV) agree fairly well with the experimental data. A rapid intersystem crossing from the excited singlet to the triplet state responsible for elimination of the fluorescence processes in these complexes may be facilitated by a high structural similarity between S_1 and T_1 as the calculations showed (see ESI, Figures S35-38).

B.3. Chiroptical properties (circular dichroism, specific and molar rotations)

The electronic circular dichroism (ECD) spectra and molar rotations (MRs) of enantiopure ligand **1a**, Pt^{II}-[8]helicene derivatives **2a**[1,2], **3a** and Pt^{II}_2-[6]helicenes **2b**[1,2], **3b** also revealed the role of the platinum centers (Table 5, Figure 3). The two *M* and *P* enantiomers of ligand **1a** with respective *ee*'s higher than 98% were obtained through HPLC separation over a chiral stationary phase (see ESI). Ligand *P*-**1a** displays the classical behaviour of a [6]helicene derivative, with a strong negative band ($\Delta\varepsilon$ = –84 $M^{-1}cm^{-1}$) at 262 nm accompanied by a smaller negative band ($\Delta\varepsilon$ = –24 $M^{-1}cm^{-1}$) at 295 nm, a strong positive band ($\Delta\varepsilon$ = +112 $M^{-1}cm^{-1}$) at 340 nm and a smaller one ($\Delta\varepsilon$ = +61 $M^{-1}cm^{-1}$) at 361 nm. Complex (*P*,S_S)-**2a**[1] displays ECD active bands that are 30–40 nm red-shifted and stronger intensity than for **1a** ((*P*,S_S)-**2a**[1]: $\Delta\varepsilon$ = +100, –91, –62, +131 $M^{-1}cm^{-1}$ at 245, 285, 325 and 374 nm respectively) together with low-energy ECD-active bands above 430 nm ((*P*,S_S)-**2a**[1]: $\Delta\varepsilon$ = +10 $M^{-1}cm^{-1}$ at 462 nm). Complex (*M*,S_S)-**2a**[2] affords nearly a mirror-image ECD spectrum of (*P*,S_S)-**2a**[1] even though this is not strictly an enantiomer pair. The ECD spectra of enantiomeric complexes *P*- and *M*-**3a** (see Figure 3 and ESI) show a similar shape to (*P*,S_S)-**2a**[1] and (*M*,S_S)-**2a**[2].

The corresponding TDDFT calculated CD envelopes agree in general well with experiment. The TDDFT electronic excitation energies, and the resulting band peaks in the simulated spectra, are somewhat blue-shifted with respect to experiment (Figures 4 and S29, ESI). As can be seen in Figure 4, important experimentally observed trends are correctly reproduced by the calculations. There is an almost uniform red-shift of the **2a**[1,2] and **3a** spectra compared to **1a**, and the CD spectra of (*P*,S_S)-**2a**[1] and (*M*,S_S)-**2a**[2] are nearly mirror images with respect to reflection on the abscissa. The ordering of intensities between **1a**, **2a**, and **3a** does not match the experiment. A strong overestimation of the main positive CD band in **1a** is in line with a too large magnitude of the calculated OR (*vide infra*). The **3a** excitation revealing the strongest rotatory strength, no. 4 (*E* = 3.66 eV, 339 nm), involves one dominant contribution (58%), from π to π* orbitals in the helicene ligand system. In terms of individual MO pairs, the transition is assigned as the HOMO-1 to LUMO (MO148 to MO150, Figures 8). Because the excitation involves orbitals centered in different parts of the ligand π-system, one can consider it as having some degree of charge transfer (CT) character. Such a CT character may be responsible for a noticeable red-shift of this excitation as compared to the corresponding excitation of **1a**, (no. 3, *E* = 3.82 eV, 324 nm, Table 2), which involves orbitals that are more uniformly spread over the helicene π-system (Figure 7). Two other CD-intense excitations of **3a** are close in energy (no. 3, 3.48 eV, 356 nm, and no. 2, 3.46 eV, 358 nm) and also exhibit a (partial) π-to-π* CT character within the helicene ligand. In both excitations the dominant contributions, 41% HOMO to LUMO+2 (MO149 to MO152) for no. 3 and 71% HOMO to LUMO+1 (MO149 to MO151) for no. 2, respectively, involve an orbital that has some visible Pt 5*d* contribution. The HOMO (MO149, Figure 4) for **3a** is similar to the HOMO (MO114) of **1a** but with some Pt character. Even though there is no obvious

π-conjugation between the metal and the pyridyl substituent (the Pt *d* lone pair orbital is oriented perpendicular to the pyridyl π-orbitals), the involvement of the metal orbital correlates with a significant increase in the rotatory strength of the **3a** transitions in comparison with the corresponding **1a** ligand. The lowest-energy **3a** excitation no. 1 calculated at E = 3.16 eV (393 nm), is assigned almost purely as HOMO to LUMO (81%). Similar to excitations no. 3 and no. 2, it is assigned as a π-to-π* transition localized in the 2-pyridyl-helicene ligand system with some participation of platinum 5*d* orbitals. Excitations that are similar in terms of energy and rotatory strength to those of **3a** are also present in the low-energy part of the CD spectrum of **2a**^{1} (compare Figure 4, Table 2, and Figure S34 in ESI).

Table 2. Selected excitations and occupied (occ) – unoccupied (unocc) MO pair contributions (greater than 10%) of *P*-**1a**, (*P*,S_S)-**2a**^{1}, and *P*-**3a**.

Excitation	E / eV	f	R / 10^{-40}cgs	occ no.	unocc no.	%
			1a			
#3	3.82	0.167	789.76	113	115	33.1
				114	116	30.4
				112	115	20.8
			2a^{1}			
#1	3.14	0.088	69.58	172	173	83.6
#3	3.52	0.017	67.04	172	174	56.3
#4	3.62	0.173	697.14	171	173	49.0
				172	174	16.7
				172	175	10.1
			3a			
#1	3.16	0.085	45.01	149	150	80.7
#2	3.46	0.029	89.37	149	151	70.6
				148	150	10.0
#3	3.48	0.021	58.90	149	152	41.3
				147	150	16.0
				148	151	15.0
				148	150	11.8
#4	3.66	0.162	649.16	148	150	58.3

Table 3. Selected excitations and occupied (occ) – unoccupied (unocc) MO pair contributions (greater than 10%) of **1b**, (P,S_S,S_S)-**2b**^{1}, and *P*-**3b**.

Excitation	E / eV	f	R / 10^{-40}cgs	occ no.	unocc no.	%
			1b			
#1	4.07	0.328	32.04	74	75	94.7
			2b^{1}			
#1	3.11	0.139	129.61	190	191	93.6
#2	3.38	0.031	-46.58	190	192	58.9
				189	191	30.9
#3	3.71	0.419	132.57	189	191	45.6
				190	192	33.3
#5[a]	3.94	0.086	-59.32	-	-	-
#10	4.36	0.023	-56.21	190	193	52.6
				189	192	29.7
#12	4.56	0.108	179.44	187	191	36.7
				190	196	21.3
			3b			
#1	3.18	0.145	126.70	144	145	92.7
#2	3.34	0.029	-70.28	144	146	57.1
				143	145	33.7
#3	3.72	0.493	122.44	143	145	52.3
				144	146	35.1
#8	4.29	0.007	80.65	144	150	43.6
				140	145	16.3
#10	4.46	0.013	-45.43	142	145	39.5
				141	146	14.4
#11	4.56	0.039	245.20	142	148	11.7

[a] No contributions exceeded 10% .

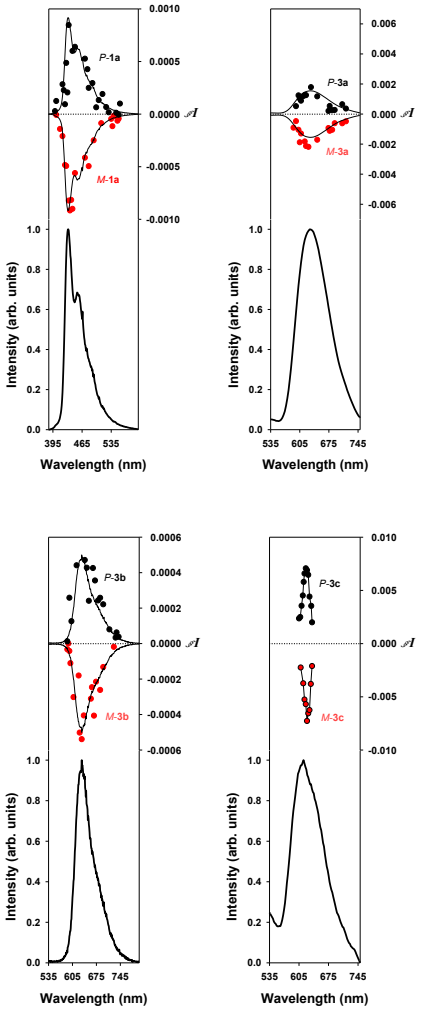

Figure 6. CPL (upper curves within each panel) and total luminescence (lower curves within each panel) spectra of *M*-**1a** (top left red), *P*-**1a** (top left black), *M*-**3a** (top right red), *P*-**3a** (top right black), *M*-**3b** (bottom left red), *P*-**3b** (bottom left black), *M*-**3c** (bottom right red), *P*-**3b** (bottom right black) in degassed dichloromethane solution (1 mM) at 295 K, upon excitation at 371-382, 452, 459-469 nm, and 452 nm respectively.

The red-shift and higher intensity of ECD-active bands for the Pt complexes is also reflected in the strong increase of the molar rotations when going from the [6]helicene ligand to the Pt-[8]helicene complexes (*P*-**1a**: +8290, (*P*,S_S)-**2a**^{1}: +19210, *P*-**3a**: +22500 (±5%) (CH_2Cl_2, *C* 10^{-4} M)). The calculated MR values agree reasonably well with the experiment (see Table 5). Although the theoretical data do not reproduce the full magnitude of the differences between the experimental optical rotations, the trend of increased optical rotation upon formation of the platinum helicenes is correctly predicted by the calculations. In line with the spatial extension of the π-conjugated systems, the MRs of both **a**-type Pt-[8]helicenecomplexes are about twice the magnitude of the parent Pt-[6]helicene **3c** derivative which itself has a MR close to the pyridyl-[6]helicene ligand **1a**. A strong over-estimation relative to the measured value (16406 *vs.* 8290 degree cm^2/dmol) was calculated for the 2-pyridyl-[6]helicene ligand **1a**. As shown in references 15, pristine and substituted helicenes can reveal a pronounced dependence of the optical rotations on their molecular structure. Inclusion of van der Waals (dispersive) forces in the geometry optimizations may be needed to improve the calculated chiroptical properties of **1a** (*vide supra*). The MR for the **2a**^{1} complex is also over-estimated by the calculations (-24008 vs. -19920 degree cm^2/dmol). The optical rotations of both **2a**^{1} and **2a**^{2} are likely to be somewhat dependent on the spatial orientation of the chiral sulfoxide ligand (in particular, the *p*-tolyl substituent) relative to the helicene π-system, due to excitonic coupling effects. Such effects have been identified and analysed previously for related metal-helicene complexes, as described in references 16. See also the discussion of the **b**-series (*vide infra*).

In the **b**-series of complexes, (*P*,S_S,S_S)-**2b**^{1} and (*P*,R_S,R_S)-**2b**^{2} display almost identical experimental CD spectra except in the 250–280 nm region (Figure 3). Their overall shape is surprisingly different from organic [6]helicene derivatives, since the strongest bands are found at 302, 350 and 371 nm with respectively $\Delta\varepsilon$ = +47, 24 and 27 $M^{-1}cm^{-1}$ only, together with several positive or negative bands between 330 and 430 nm of even lower intensities. The CD spectrum of *P*-**3b** shows an overall similar behaviour, with a set of one rather strong negative bands ($\Delta\varepsilon$ = –85 $M^{-1}cm^{-1}$) at 243 nm, one strong positive band ($\Delta\varepsilon$ = +107 $M^{-1}cm^{-1}$) at 293 nm, and four moderately intense positive bands ($\Delta\varepsilon$ = +14, 22, 8, 21 $M^{-1}cm^{-1}$ at 342, 374, 443, 468 respectively). As Figures 4 and S30-32 (ESI) show, the calculated spectral envelopes of complexes **2b**^{1,2} and **3b** agree generally quite well with experiment, provided that a red-shift is applied to the calculated spectra. In accordance with experiment, complexes **2b**^{1} and **3b** display positive CD bands of significant intensity in the low-energy part of the spectra (excitation no. 1, *E* = 3.11 eV (399 nm) and 3.18 eV (390 nm) for **2b**^{1} and **3b**, respectively) that are of almost pure HOMO-to-LUMO character (**2b**^{1}: MO190 to MO191: 94%, Figure 9, and **3b**: MO144 to MO145: 93%, Figure 10) correspond to π-to-π* transition localized in the pyridyl-based helicene moiety with slight, but not negligible, involvement of platinum orbitals this sentence is not clear to me. The next excitation, no. 2, calculated at *E* = 3.38 eV, 366 nm (**2b**^{1}) and 3.34 eV, 371 nm (**3b**) has a negative rotatory strength and consequently suppresses positive band intensity at the low-energy spectral region for both compounds. For both **2b**^{1} and **3b** this excitation is a π-to-π* transition localized in the pyridyl-based helicene moiety with participation of Pt 5*d* orbitals (HOMO to LUMO+1: ~ 58% and HOMO-1 to LUMO: ~ 33%, see Figures 9, 10). Unlike HOMO-1 for **2**,**3a** which are localized predominantly on the carbohelical fragment, the corresponding orbitals of **2**,**3b** show a noticeable contribution from lone pairs of both platinum centers which become a part of the naphthalene π-system, along with non-negligible participation of the acetylacetonate (acac) ligand moieties. Excitations no. 3 (3.71 eV, 334 nm for **2b**^{1} and 3.72 eV, 333 nm for **3b**) have qualitatively the same assignment as no. 2, with two main contributions, HOMO to LUMO+1 and HOMO-

1 to LUMO but more weight on the latter (46% for **2b**[1] and 52% for **3b** versus 33% and 35%, respectively). The HOMO to LUMO+1 orbital pair indicates a degree of CT character in the excitation as it involves orbitals centered in different parts of the ligand π-system.

Table 4. Experimental and calculated photophysical data of ligand **1a** and of the mono- and bis-cycloplatinated helicenes **3a**,**b**,**c**. Energies in eV.

System	*P*-**1a**	*P*-**3a**	*P*-**3b**	*P*-**3c**
Experiment Emission 298 K [a]	2.88, 2.74	1.91	1.96, 1.84	1.93
Emission 77 K [a]	2.95, 2.78, 2.62, 2.46 (fluo) 2.29, 2.10, 1.94 (phos)	2.07, 1.93	2.04, 1.87, 1.71	2.09, 1.94, 1.79
BHLYP/SV(P)				
$S_1^{\{TDDFT\}b}$	2.93 (0.0477 / 390.92)	2.88 (0.1044 / 55.84)	2.95 (0.1399 / 106.02)	2.92 (0.1524 / 6.75)
$T_1^{\{TDDFT\}c}$	1.63	1.90	1.92	1.89
$T_1^{\{DFT\}d}$	1.76	1.89	1.93	1.89
$S_0//T_1^{\{DFT\}}$ - $T_1//T_1^{\{DFT\}e}$	1.70	1.81	1.93	1.80
CASSCF				
$T_1^{\{DFT\}f}$	1.68 (0.00 / 0.00)	-	-	2.11 ($1.31\cdot10^{-6}$ / $9.19\cdot10^{-5}$)
CASPT2				
$T_1^{\{DFT\}g}$	2.42 (0.00 / 0.00)	-	-	2.05 ($1.35\cdot10^{-5}$ / $1.57\cdot10^{-3}$)

[a] Experimental data. [b] TDDFT S_0-S_1 energy difference at TDDFT BHLYP/SV(P) optimized S_1 geometry. In parentheses oscillator strength, in au / rotatory strength values, in 10^{-40} cgs, are listed. To convert to integrated CPL intensity, in cgs units of power output per molecule, the following conversion can be used: $\Delta I = 1.60041320\cdot10^{37}\cdot R_{cgs}\cdot E_{cgs}^{4}$.[c] TDDFT S_0-T_1 energy difference at TDDFT BHLYP/SV(P) optimized T_1 geometry.[d] TDDFT S_0-T_1 energy difference at DFT BP/SV(P) optimized triplet configuration.[e] S_0-T_1 energy gap calculated as difference between $S_0//T_1^{\{DFT\}}$ and $T_1//T_1^{\{DFT\}}$.[f/g] Spin-orbit CASSCF / CASPT2[14] S_0-T_1 energy differences at DFT BP/SV(P) optimized triplet configuration, and corresponding intensities. See ESI for calculations details. See also footnote b.

Table 5. Experimental and calculated optical rotations for the [6]helicene ligand **1a** and mono- and bis-cycloplatinated helicenes **2a,b**[1,2] and **3a,b**. [a)]

	BHLYP/SV(P)		Expt. (23°C)
	$[\alpha]_D$	$[\phi]_D$	$[\phi]_D$
P-**1a**	3767	16406	8290
(*M*,R_S)-**2a**[1]	-2930	-24008	-19920
(*P*,R_S)-**2a**[2]	2337	19147	19210
P-**3a**	3197	23298	22500
(*P*,S_S,S_S)-**2b**[1]	933.4	9800	11720
(*P*,R_S,R_S)-**2b**[2]	413.1	4337	9616
P-**3b**	1185	10297	8950
P-**3c**[b)]	1588	9982	8170

[a)] Specific rotations and molar rotations are given in the usual units of degree/(dm g/cm^{-3}) and degree cm^2/dmol, respectively. [b)] Data from references 4a,b.

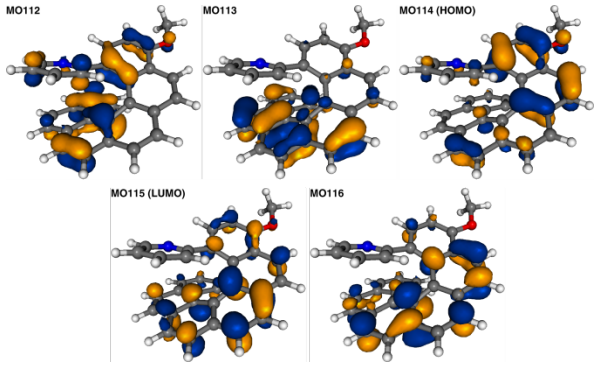

Figure 7. Isosurfaces (0.04 au) of MOs involved in selected excitations of **1a**.

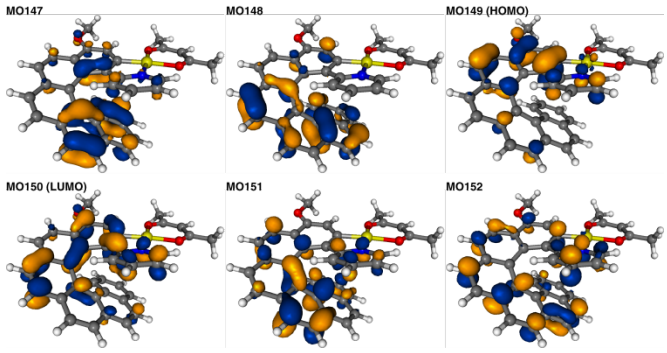

Figure 8. Isosurfaces (0.04 au) of MOs involved in selected excitations of **3a**.

Despite some unique features of the **2**,**3b** CD spectra, the experimental molar rotation values are typical for [6]helicene derivatives (complexes (*P*,S_S,S_S)-**2b**[1]: $[\phi]_D^{23}$ = +11720,(*P*,R_S,R_S)-**2b**[2]: +9616, *P*-**3b**: +8950 (±5%) (in CH_2Cl_2 solution at 10^{-4} M)) and of same order of magnitude as the MR of *P*-**3c** (Table 5). We attribute this to the similar sizes of the helical π-systems. Satisfactory agreement of calculated ORs with experiment is found for all the systems except **2b**[2] for which a striking underestimation occurs (4337 vs. 9616 degree cm^2/dmol, see Table 5). Due to this discrepancy, a series of additional calculations were carried out to study possible influences of density functional, basis set as well as an effect of structural parameters on the calculated MR (see ESI, Tables S1 and S2,and Figures S31-S33). As indicated above, the orientation of the sulfoxide ligand has a strong effect on the calculated optical rotation values which we tentatively attribute to excitonic effects similar to those described in references 16.

A comparison of the CD spectra of the ligand **1a** and complexes **3a-c** as depicted in Figure 5 highlights their common and different general features: *i*) the CD spectra of the organic 2-pyridyl-[6]helicene **1a** and organometallic Pt-[6]helicene **3c** display similar overall shape; *ii*) Pt-[8]helicene **3a** displays a stronger and more red-shifted CD spectrum compared to Pt-[6]helicene **3c**, a well-known tendency for helicenes that can be attributed to an enlargement of the π-electron system; *iii*) Pt_2-[6]helicene **3b** displays a significantly different CD spectrum from **3a**,**c** and **1a**. The TDDFT results

indicate that this is due to a cancellation of CD-active transitions with opposite sign rotatory strengths and similar energies.

B.4. Circularly polarized luminescence (CPL)

We have resorted to CPL, the emission analogue of ECD, to further investigate the influence of the helicity in the compounds of interest on the chiroptical properties. The circularly polarized luminescence (ΔI) and total luminescence (I) spectra measured for *P*-/*M*-**1a**, *P*-/*M*-**3a**, *P*-/*M*-**3b**, and *P*-/*M*-**3c** in dichloromethane solutions at 295 K are shown in Figure 6, respectively. The degree of circularly polarized luminescence is given by the luminescence dissymmetry ratio, $g_{lum}(\lambda) = 2\Delta I/I = 2(I_L - I_R)/(I_L + I_R)$, where I_L and I_R refer, respectively, to the intensity of left and right circularly polarized emissions.[17] The solid lines in the CPL plot are presented to show the luminescence spectral line shape.

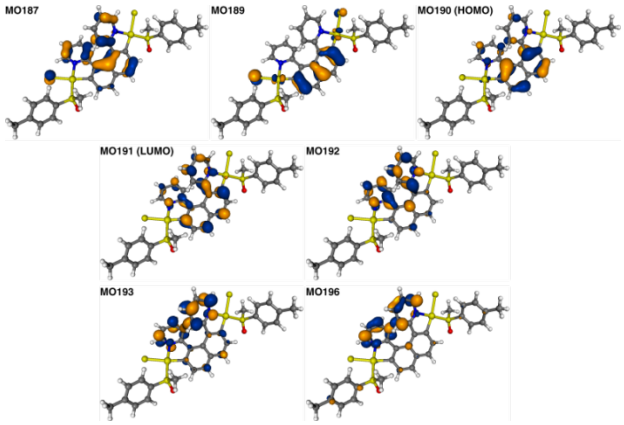

Figure 9. Isosurfaces (0.04 au) of MOs involved in selected excitations of **2b**[1].

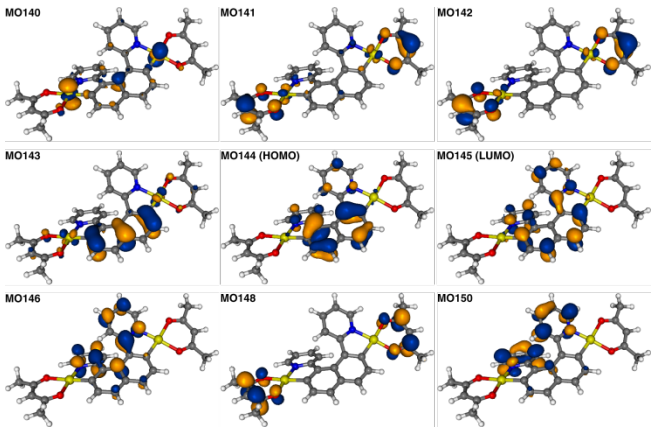

Figure 10. Isosurfaces (0.04 au) of MOs involved in selected excitations of **3b**.

As usual for most chiral organic chromophores and transition metal complexes, the $|g_{lum}|$ values obtained are small: –0.0008/+0.0008, –0.0050/+0.0040, –0.0005/+0.0005 and –0.011/+0.013 for *M*-**1a**/*P*-**1a**, *M*-**3a**/*P*-**3a**, *M*-**3b**/*P*-**3b**and *M*-**3c**/*P*-**3c** respectively, as determined at their maximum emission wavelengths. Although these g_{lum} values are very small (a value equal to ~0.004 corresponding to light that is only 0.4% circularly polarized), opposite CPL signals were measured for the four sets of compounds having opposite *P* and *M* helical configuration. These results confirm that the organic and organometallic helicene solutions in dichloromethane exhibit an active CPL signal and the emitted light is polarized in opposite directions for the two enantiomeric forms for each set of these helicenes. Overall, the experimental $|g_{lum}|$ values are similar to the ones obtained for organic helicenes,[3a,18] except for Pt-[6]helicene which displays a higher $|g_{lum}|$ value of the order 10^{-2}, the biggest value obtained for molecular helicenes.[3b,d] It must be pointed out that the CPL activity is dependent on the structural properties of the compounds of interest is it really necessary to say that?. Of special importance is that the addition of the Pt fragment in only three steps resulted in the formation of organometallic helicenes that possessed a CPL activity more efficient than their organic counterparts (|0.01| *vs.* |0.0008|), even if Pt is not a stereogenic center in these platinahelicene derivatives (a square planar geometry around the Pt centre is observed). Notably, compared to former CPL active helicenes that are fluorescent organic systems, these are phosphorescent. As already mentioned, phosphorescence of these helicene derivatives comes from the presence of the heavy platinum atom which has a large spin-orbit coupling constant. Interestingly, although the platinum center is non-chiral in itself, it provides helicenes with circularly polarized phosphorescence. This can be explained by the fact that the platinum orbitals are conjugated within the π-system of the helical ligand. The quantum-chemical calculations discussed above confirm participation of Pt 5d orbitals in the MOs that contribute to the electronic transitions. Additional preliminary calculations of spectral emission properties were carried out for **1a** and **3c** (Table 4) with complete active space self-consistent field (CASSCF) and complete active space second-order perturbation theory (CASPT2) including spin-orbit coupling effects (see ESI).[14] A full account of calculated emission spectra will be given in a follow-up publication. The dependence of the wave-function based results on the size of the active spaces needs to be investigated in more detail. However, the preliminary calculations confirm that the CD of the S_0-S_1 excitation of *P*-**1a** and the CPL of the S_1-S_0 emission have the same sign. For *P*-**3c**, calculations at the optimized structure of T_1 at different levels of theory including spin-orbit coupling predict nonzero positive rotatory strengths for the T_1-S_0 emission, which is also consistent with the sign of the CPL in the experiment. The smaller CPL activity of the bis-platinated[6]helicene **3b** compared to its mono-platinated helicene[6] analogue **3c** (|0.0005| *vs.* |0.01|) seen experimentally is probably a consequence of two factors: (*i*) weaker ECD active bands and stronger UV-vis bands involving the platinum centres, (*ii*) a possibility of racemization of **3b** under irradiation by the xenon lamp used for CPL measurements. This is in line with the fact that the CPL response is influenced by the chiral arrangement surrounding the luminescent centre.[17a,b]

C Conclusions

We have developed an efficient crystallization process combined with chromatography of diastereomeric cycloplatinated complexes bearing a chiral sulfoxide ligand to obtain unprecedented enantiopure mono- and bis-platinahelicenes bearing respectively an [8] and a [6]helicenic backbone. The easy access to these enantiopure cycloplatinated helicenes enabled us to examine the influence of different structural features on the UV-visible spectra, circular dichroism, molar rotations, luminescence and CPL activity. It was shown that, although the platinum center is not a stereogenic element, these platinahelicenes displayed circularly polarized phosphorescence, with highest g_{lum} values of the order of 10^{-2}.

Acknowledgements

We thank the Ministère de l'Education Nationale, de la Recherche et de la Technologie, the Centre National de la Recherche Scientifique (CNRS) and the ANR (12-BS07-0004-METALHEL-01) and the LIA Rennes-Durham for financial support. The theoretical component of this work has received financial support from the National Science Foundation (CHE 0952253, CHE 1265833 to J.A.) and the Foundation for Polish Science Homing Plus programme co-financed by the European Regional Development Fund under the Operational Programme Innovative Economy (to M. S.). M. S. is also grateful for financial support from the Ministry of Science and Higher Education in Poland ('Outstanding Young Scientist' scholarship). M. S. and J. A. acknowledge the Center for Computational Research (CCR) at the University at Buffalo for providing computational resources. G.M. thanks the National Institute of Health, Minority Biomedical Research Support (1 SC3 GM089589-03 and 3 S06 GM008192-27S1) and the Henry Dreyfus Teacher-Scholar Award for financial support, whilst T. D. J. and K. K. D. thank the NIH (RISE Grant 5R25GM071381 and MARC Grant XXX, respectively) for research fellowships.

Notes and references

[a] Institut des Sciences Chimiques de Rennes, UMR 6226, Institut de Physique de Rennes, UMR 6251, Campus de Beaulieu, CNRS-Université de Rennes 1, 35042 Rennes Cedex, France. E-mail: jeanne.crassous@univ-rennes1.fr

[b] Faculty of Chemistry, Jagiellonian University, 30-060 Krakow, Poland.

[c] Chirosciences, UMR 7313, Stéréochimie Dynamique et Chiralité, Aix-Marseille University, 13397 Marseille Cedex 20, France.

[d] Department of Chemistry, San José State University, San José, CA 95192-0101, USA.

[e] Department of Chemistry, University of Durham, Durham, DH1 3LE, UK.

[f] Department of Chemistry, University at Buffalo, State University of New York, Buffalo, NY 14260, USA.E-mail: jochena@buffalo.edu

Electronic Supplementary Information (ESI) available: experimental procedures, fluorescence and phosphorescence emission and excitation spectra, X-ray data, theoretical calculations details. See DOI: 10.1039/b000000x/

1 Selected reviews, see: (a) Y. Shen, C. -F. Chen, *Chem. Rev.* 2012, **112**, 1463 and references therein. (b) M. Gingras, *Chem. Soc. Rev.,* 2013, **42**, 1051. (c) I.G. Stará, I. Starý, in: J.S. Siegel, Y. Tobe (Eds.), *Science of Synthesis*, vol. 45, Thieme, Stuttgart (2010), pp. 885-953. (d) A. Rajca, M. Miyasaka, in *Functional Organic Materials* (Eds.: Müller, T.J.J.; Bunz, U. H. F.), Wiley-VCH, Weinheim, 2007, pp. 543-577. (e) A. Urbano, *Angew. Chem. Int. Ed*., 2003, **42**, 3986. (f) T.J. Katz, *Angew. Chem. Int. Ed*., 2000, **39**, 1921. (g) R.H. Martin, *Angew. Chem. Int. Ed*.,1974, **13**, 649.

2 (a) D. Amabilino, *Chirality at the Nanoscale, Nanoparticles, Surfaces, Materials and more*, Wiley-VCH, 2009. (b) B.L. Feringa, W.R. Browne, *Molecular Switches*, Wiley-VCH, 2001.

3 Selected examples: (a) J.E. Field, G. Muller, J.P. Riehl, D. Venkataraman, *J. Am. Chem. Soc.,*2003, **125**, 11808. (b) Y. Sawada, S. Furumi, A. Takai, M. Takeuchi, K. Noguchi, K. Tanaka, *J. Am. Chem. Soc*., 2012, **134**, 4080. (c) K.E. S. Phillips, T.J. Katz, S. Jockusch, A.J. Lovinger, N.J. Turro, *J. Am. Chem. Soc.,*2001, **123**, 11899. (d) T. Kaseyama, S. Furumi, X. Zhang, K. Tanaka, M. Takeuchi, *Angew. Chem., Int. Ed*., 2011, **50**, 3684. (e) E. Anger, M. Srebro, N. Vanthuyne, L. Toupet, S.Rigaut, C. Roussel, J. Autschbach, J. Crassous, R. Réau, *J. Am. Chem. Soc.,* 2012, **134**, 15628. (f) J. Nishida, T. Suzuki, M. Ohkita, T. Tsuji, *Angew. Chem. Int. Ed.,*2001, **40**, 3251. (g) T. Biet, A. Fihey, T. Cauchy, N. Vanthuyne, C. Roussel, J. Crassous, N. Avarvari, *Chem. Eur. J.,* 2013, **19**, 13160. (h) C.-T. Chen, C.-H. Chen, T.-G.Ong, *J. Am. Chem. Soc.,*2013, **135**, 5294. (i) T.J.Wigglesworth, D. Sud, T.B. Norsten, V.S. Lekhi, N.R. Branda, *J. Am. Chem. Soc.,*2005, **127**, 7272. (j) T. Hatakeyama, S. Hashimoto, T. Oba, M. Nakamura M. *J. Am. Chem. Soc.,* 2012, **134**, 19600. (k) Y. Yang, R.C. da Costa, M.J. Fuchter, A.J. Campbell, *Nature Photonics,* 2013, **7**, 634. (l) T. Verbiest, S. Van Elshocht, M. Kauranen, L. Hellemans, J. Snauwaert, C. Nuckolls, T J. Katz, A. Persoons, *Science,* 1998, **282**, 913.

4 (a) L. Norel, M. Rudolph, N. Vanthuyne, J.A.G. Williams, C. Lescop, C. Roussel, J. Autschbach, J. Crassous, R. Réau, *Angew. Chem. Int. Ed.,* 2010, **49**, 99. (b) E. Anger, M. Rudolph, L. Norel, S. Zrig, C. Shen, N. Vanthuyne, L. Toupet, J.A.G. Williams, C. Roussel, J. Autschbach, J. Crassous, R. Réau, *Chem. Eur. J.*, 2011, **17***,* 14178. (c) E. Anger, M. Rudolph, C. Shen, N. Vanthuyne, L. Toupet, C. Roussel, J. Autschbach, J. Crassous, R. Réau, *J. Am. Chem. Soc.*, 2011, **133***,* 3800. (d) C. Shen, E. Anger, M. Srebro, N. Vanthuyne, L. Toupet, C. Roussel, J. Autschbach, R. Réau, J. Crassous, *Chem. Eur. J.,* 2013, **19**, 16722. (e) O. Crespo, B. Eguillor, M.A. Esteruelas, I. Fernandez, J. Garcia-Raboso, M. Gomez-Gallego, M. Martin-Ortiz, M. Olivan, M.A. Sierra, *Chem. Comm*., 2012, **48**, 5328.

5 Selected examples: (a) M. Gingras, *Chem. Soc. Rev*., 2013, **42**, 1007. (b) B. Laleu, P. Mobian, C. Herse, B. W. Laursen, G. Hopfgartner, G. Bernardinelli, J. Lacour, *Angew. Chem. Int. Ed.,* 2005, **44**, 1879. (c) B. Heller, M. Hapke, C. Fischer, A. Andronova, I. Stary, I. G. Stara, *J. Organomet. Chem*., 2013, **723**, 98 and references therein. (d) Y. Sawada, S. Furumi, A. Takai, M. Takeuchi, K. Noguchi, K. Tanaka, *J. Am. Chem. Soc*., 2012, **134**, 4080. (e) A. Latorre, A. Urbano, C. M. Carreno, *Chem. Comm*., 2011, **47**, 8103. (f) M. Weimar, R. Correa da Costa, F.-H. Lee, M.J. Fuchter, *Org. Lett.*, 2013, **15**, 1706. (g) K.

Yavari, S. Moussa, B. Ben Hassine, P. Retailleau, A. Voituriez, A. Marinetti, *Angew. Chem. Int. Ed*., 2012, **51**, 6748. (h) J. Zadny, A. Jancarik, A. Andronova, M. Samal, J.V. Chocholousova, J. Vacek, R. Pohl, D. Saman, I. Cisarova, I.G. Stara, I. Stary, *Angew. Chem. Int. Ed*., 2012, **51**, 5857.

6 (a) J. Jacques, A. Collet and S. H. Wilen*, Enantiomers, Racemates, and Resolutions*, Krieger, Malabar, Florida, 2nd ed., 1994. (b) See J. Vavra, L. Severa, I. Cisarova, B. Klepetarova, D. Saman, D. Koval, V. Kasicka, F. Teply, *J. Org. Chem*., 2013, **78**, 1329 and references therein. (c) J. Vavra, L. Severa, P. Svec, I. Cisarova, D. Koval, P. Sazelova, V. Kasicka, F.Teply, *Eur. J. Org. Chem.,* 2012, 489. (d)K. Paruch, T.J. Katz, C. Incarvito, K.C. Lam, B. Rhatigan, A.L. Rheingold, *J. Org. Chem*., 2000, **65**, 7602. (e) M.S. Newman, D. Lednicer,*J. Am. Chem. Soc*., 1956, **78**, 4765.

7 (a) M.. Kobayashi, S. Masaoka, K. Sakai, *Acta Cryst.,* 2008, **E64**, 1325. (b) A. Santoro, A.C. Whitwood, J.A.G. Williams, V.N. Kozhevnikov, D.W. Bruce, *Chem. Mater.,* 2009, **21**, 3871. (c) A. Santoro, M. Wegrzyn, A.C. Whitwood, B. Donnio, D.W. Bruce, *J. Am. Chem. Soc.,* 2010, **132**, 10689.

8 (a) A.D. Ryabov, I.M. Panyashkina, V.A. Polyakov, J.A.K. Howard, L.G. Kuz'mina, M.S. Datt, C. Sacht, *Organometallics* , 1998, **17**, 3615.(b) K. Suenkel, R. Branzan, S. Weigand, *Inorg. Chim.Acta* , 2013, **399**, 193. (c) J.-P. Djukic, A. Hijazi, H.D. Flack, G. Bernardinelli, *Chem. Soc. Rev*., 2008, **37**, 406.

9 (a) G. Pieters, A. Gaucher, D. Prim, J. Marrot, *Chem. Comm*., 2009, 4827. (b) J.A. Zoltewicz, N.M. Maier, *J. Org. Chem*., 1997, **62**, 3215. (c) X. Mei, R.M. Martin, C. Wolf, *J. Org. Chem.,* 2006, **71**, 2854. (d) S. Vyskocil, L. Meca, I. Tislerova, I. Cisarova, M. Polasek, S.R. Harutyunyan, Y.N. Belokon, R.M.J. Stead, L. Farrugia, S.C. Lockhart, W.L. Mitchell, P. Kocovsky, *Chem. Eur. J*., 2002, **8**, 4633. (e) C. Wolf, X. Mei, *J. Am. Chem. Soc*., 2003, **125**, 10651.

10 Example of diastereoselective cycloplatination reaction, see: (a) H. Huang, R. Peters, *Angew. Chem. Int. Ed*., 2009, **48**, 604. Examples of chiral platinated complexes: (b) C. Anderson, M. Crespo, J. Morris, J. M. Tanski, *J. Organomet. Chem.,* 2006, **691**, 5635. (c) M. R. Plutino, L. MonsuScolaro, A. Albinati, R. Romeo, *J. Am. Chem. Soc.,* 2004, **126**, 6470. (d) M.E. Günay, D.L. Hughes, C.J. Richards, *Organometallics,* 2011, **30**, 3901.(e) C. Lopez, A. Caubet, S. Perez, X. Solans, M. Font-Bardia, *Chem. Comm.,* 2004, 540.

11 (a) M. Valiev, E. Bylaska, N. Govind, K. Kowalski, T. Straatsma, H. V. Dam, D. Wang, J. Nieplocha, E. Apra, T. Windus, W. de Jong, *Comput. Phys. Commun*., 2010, **181**, 1477. (b) S. Hirata, C.-G. Zhan, E. Aprà, T.L. Windus, D.A. Dixon, *J. Phys. Chem. A,* 2003, **107**, 10154. (c) J. Autschbach, *ChemPhysChem,* 2011, **12**, 3224.

12 (a) V.N. Kozhevnikov, M.C. Durrant, J.A.G. Williams, *Inorg. Chem.,* 2011, **50**, 6304. (b) S. Culham, P.-H. Lanoë, V.L. Whittle, M.C. Durrant, J.A.G. Williams, V.N. Kozhevnikov, *Inorg. Chem.,* 2013, **52**, 10992.

13 (a) A.Y.-Y. Tam, D.P. -K. Tsang, M.Y. Chan, N.Y. Zhu, V.W.-W. Yam, *Chem. Commun.* 2011, **47**, 3383. (b) C. A. Strassert, C.-H. Chien, M.D. Galvez Lopez, D. Kourkoulos, D. Hertel, K. Meerholz, L. De Cola, *Angew. Chem. Int. Ed.* 2011, **50**, 946.(c) W. Mroz, C. Botta, U. Giovanella, E. Rossi, A. Colombo, C. Dragonetti, D. Roberto, R. Ugo, A. Valore, J.A.G. Williams, *J. Mater. Chem.,* 2011, **21**, 8653. (d) E. Rossi, L. Murphy, P.L. Brothwood, A. Colombo, C. Dragonetti, D. Roberto, R. Ugo, M. Cocchi, J.A.G. Williams, *J. Mater. Chem*., 2011, **21**, 15501. (e) S.C.F. Hui, P.K. Chow, G.S.M. Tong, S.-L. Lai, G. Cheng, C.-C. Kwok, K.-H. Low, M.Y. Ko, C.-M. Che, *Chem. Eur. J.,* 2013, **19**, 69. (f) J. Zhang, F.C. Zhao, X.J. Zhu, W.-K. Wong, D.G. Ma, W.-Y. Wong, *J. Mater. Chem.,* 2012, **22**, 16448. (g) X.-C. Hang, T. Fleetham, E. Turner, J. Brooks, J. Li, *Angew. Chem. Int. Ed.,* 2013, **52**, 6753. (h) E. Turner, N. Bakken, J. Li, *Inorg. Chem.,* 2013, **52**, 7344.

14 F. Aquilante, L. De Vico, N. Ferré, G. Ghigo, P.-Å. Malmqvist, P. Neogrády, T.B. Pedersen, M. Pitoňák, M. Reiher, B. O. Roos, L. Serrano-Andrés, M. Urban, V. Veryazov, R. Lindh, *J. Comput. Chem*., 2010, **31**, 224.

15 (a) M. Srebro, N. Govind, W.A. de Jong, J. Autschbach, *J. Phys. Chem. A*, **2011**, *115*, 10930. (b) M. El Sayed Moussa, M. Srebro, E. Anger, N. Vanthuyne, C. Roussel, C. Lescop, J. Autschbach, J. Crassous, *Chirality*, 2013, **25**, 455.

16 (a) S. Graule, M. Rudolph, N. Vanthuyne, J. Autschbach, C. Roussel, J. Crassous, R. Réau, *J. Am. Chem. Soc*., 2009, **131**, 3183. (b) S. Graule, M. Rudolph, W. Shen, C. Lescop, J.A.G. Williams, J. Autschbach, J. Crassous, R. Réau, *Chem. Eur. J*., 2010, **16**, 5976.

17 (a) *Circularly Polarized Luminescence Spectroscopy and Emission-Detected Circular Dichroism;* J. P. Riehl, G. Muller, In *Comprehensive Chiroptical Spectroscopy*, First Edition, Ed. N. Berova, P.L. Polavarapu, K. Nakanishi, R.W. Woody, John Wiley & Sons, Inc.: Hoboken, New Jersey, 2012, Vol. 1: Instrumentation, Methodologies, and Theoretical Simulations, Chapter 3, pp. 65-90. (b) K.M. Solntsev, E.-A. Gould, G. Pan, G. Muller, S. Bommireddy, D. Huppert, L.M. Tolbert, *Isr. J. Chem.*, 2009, **49**, 227. (c) *Circularly Polarized Luminescence Spectroscopy from Lanthanide Systems;* J.P. Riehl, G. Muller, In *Handbook on the Physics and Chemistry of Rare Earths*, ed. K.A. Gschneidner, Jr., J.-C.G. Bünzli, V.K. Pecharsky, North-Holland Publishing Company: Amsterdam,2005, Vol. 34, Chapter 220, pp.289-357, and references therein.

18 For different examples of CPL active helicenes see ref. 3a-d and (a) Y. Tang, T.A. Cook, A.E. Cohen, *J. Phys. Chem. A.,* 2009, **111**, 6213. (b) K. Goto, R. Yamaguchi, S. Hiroto, H. Ueno, T. Kawai, H. Shinokubo, *Angew. Chem. Int. Ed.,* 2012, **51**, 10333. (c) A. Cyphersmith, S. Surampudi, M.J. Casey, K. Jankowski, D. Venkataraman, M.D. Barnes, *J. Phys. Chem. A.,*2012, **116**, 5349. (d) Y. Yang, R.C. da Costa, D.-M. Smilgies, A.J. Campbell, M.J. Fuchter, *Adv. Mater.,* 2013, **15**, 2624.